Supporting Information

Revealing the roles of solid-electrolyte interphase in designing stable, fast-charging, low-temperature Li-ion batteries

Lei Tao[1,a], Hanrui Zhang[2,a], Sameep Rajubhai Shah[3,a], Xixian Yang[3], Jianwei Lai[2], Yanjun Guo[2], Joshua A. Russell[4], Dawei Xia[1], Jungki Min[1], Weibo Huang[1], Chenguang Shi[1], Zhaohui Liang[1], Deyang Yu[1], Sooyeon Hwang[5], Hui Xiong[4], Louis A. Madsen[1,6], Kejie Zhao[3], Feifei Shi[2*], Feng Lin[1,6,7*]*

[1]Department of Chemistry, Virginia Tech, Blacksburg, VA 24061, USA

[2]Department of Energy and Mineral Engineering, Pennsylvania State University, University Park, PA 16802, USA

[3]School of Mechanical Engineering, Purdue University, West Lafayette, IN 47907, USA

[4]Micron School of Materials Science and Engineering, Boise State University, Boise, ID 83725, USA

[5] Center for Functional Nanomaterials, Brookhaven National Laboratory, Upton, NY 11973, USA

[6] Macromolecules Innovation Institute, Virginia Tech, Blacksburg, VA 24061, USA

[7] Department of Materials Science and Engineering, Virginia Tech, Blacksburg, VA 24061, USA

[*]Corresponding: kjzhao@purdue.edu; feifeishi@psu.edu; fenglin@vt.edu;

[a] These authors contributed equally to this work.

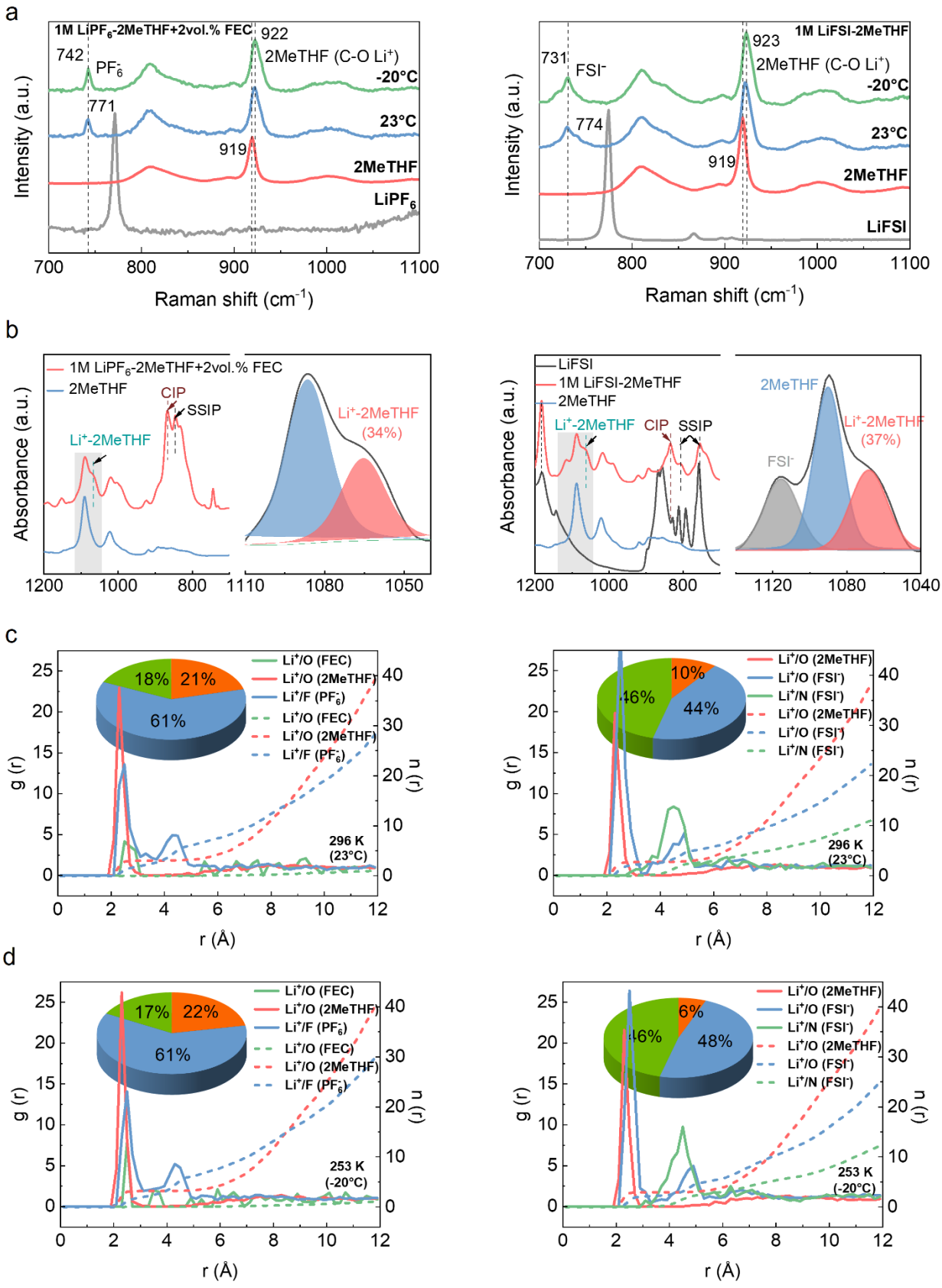
a
1M LiPF6-2MeTHF+2vol.% FEC
742
PF6-
771
922
2MeTHF (C-O Li+)
919
-20°C
23°C
2MeTHF
LiPF6
Intensity (a.u.)
Raman shift (cm-1)
1M LiFSI-2MeTHF
731
FSI-
774
923
2MeTHF (C-O Li+)
919
-20°C
23°C
2MeTHF
LiFSI
Intensity (a.u.)
Raman shift (cm-1)
b
1M LiPF6-2MeTHF+2vol.% FEC
2MeTHF
CIP
SSIP
Li+-2MeTHF
Li+-2MeTHF (34%)
Absorbance (a.u.)
LiFSI
1M LiFSI-2MeTHF
2MeTHF
Li+-2MeTHF
CIP
SSIP
2MeTHF
Li+-2MeTHF (37%)
FSI-
Absorbance (a.u.)
c
18%
21%
61%
Li+/O (FEC)
Li+/O (2MeTHF)
Li+/F (PF6-)
296 K (23°C)
g (r)
n (r)
r (Å)
10%
46%
44%
Li+/O (2MeTHF)
Li+/O (FSI-)
Li+/N (FSI-)
296 K (23°C)
g (r)
n (r)
r (Å)
d
17%
22%
61%
Li+/O (FEC)
Li+/O (2MeTHF)
Li+/F (PF6-)
253 K (-20°C)
g (r)
n (r)
r (Å)
6%
46%
48%
Li+/O (2MeTHF)
Li+/O (FSI-)
Li+/N (FSI-)
253 K (-20°C)
g (r)
n (r)
r (Å)

Fig. S1. Electrolytes properties at different temperatures. **a**, Raman spectra of the electrolytes (1M $LiPF_6$-2MeTHF+2vol.% FEC, 1M LiFSI-2MeTHF) at 23 and -20°C, with $LiPF_6$, LiFSI, and 2MeTHF reference spectra included. As the temperature decreases, the representative peaks have not shifted. **b**, FTIR spectra of the electrolytes at 23°C. In the fitted curves, blue represents free 2MeTHF solvent, and red represents solvated Li^+ (Li^+-2MeTHF). The proportions of solvated Li^+ in different electrolytes are 34%, and 37%, respectively (from left to right figure). **c, d**, Radial distribution function (RDF, g(r), solid) and coordination number (CN, n (r), dashed line) of oxygen and fluorine around Li^+ as a function of distance (r) from MD simulations in the electrolytes at 296 K (23°C) and 253K (-20°C), respectively. The insert figures refer to the statistical analysis of the Li^+ solvates (SSIP (orange), CIP (blue), and AGG (green)) in the electrolytes from MD simulations.

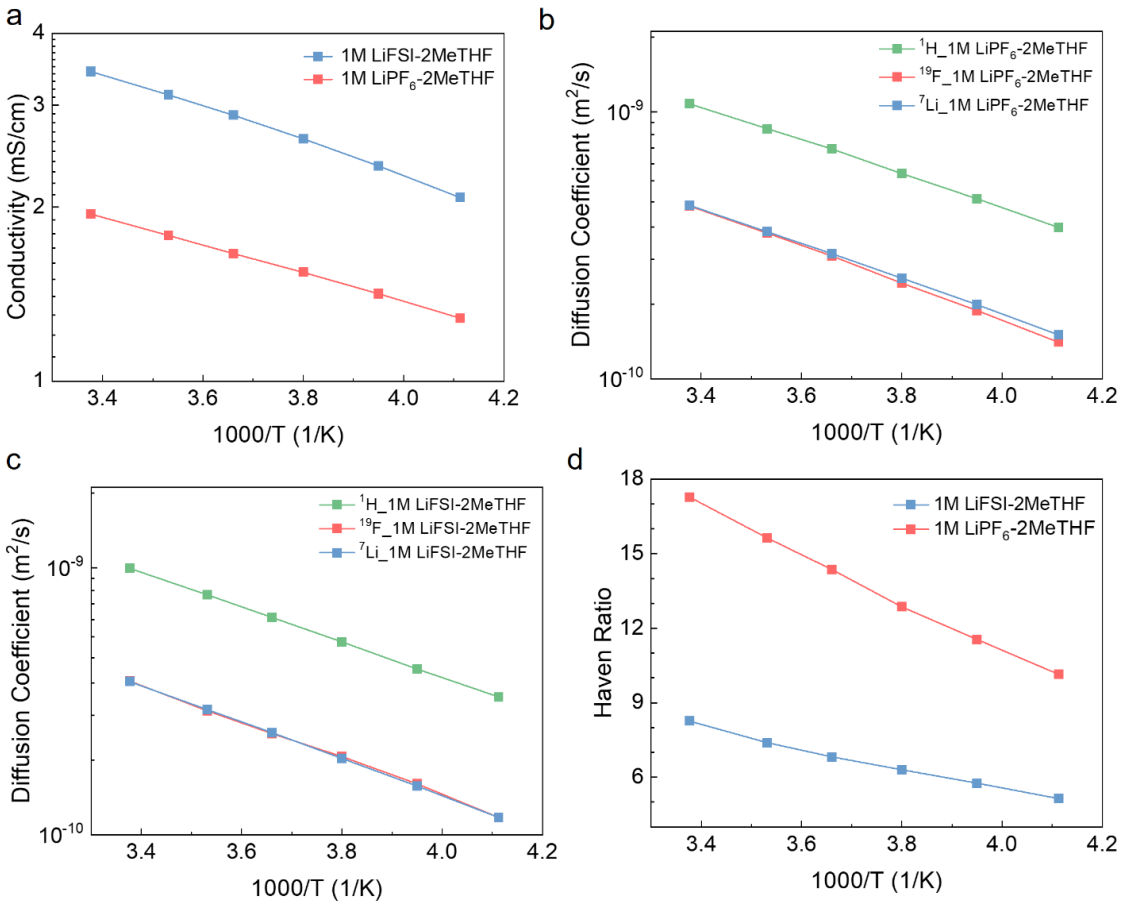

Fig. S2. a, Conductivities of the electrolytes in the temperature range of 20 to -30°C. **b**, Diffusion coefficients of the cation (Li^+), anion (PF_6^-), and solvent (2MeTHF) in 1M $LiPF_6$-2MeTHF. **c,** Diffusion coefficients of the cation (Li^+), anion (FSI^-), and solvent (2MeTHF) in 1M LiFSI-2MeTHF. **d**, Haven ratios of the electrolytes as a function of temperature. The conductivity of the electrolytes was measured using an electrophoretic NMR cell, and the cell constant was calibrated using a standard KCl solution.[12]

Fig. S2a shows that the conductivity of 1M LiFSI-2MeTHF is slightly higher than that of the 1M $LiPF_6$-2MeTHF electrolyte. However, the self-diffusion coefficients of Li^+ and the anion in 1M LiFSI-2MeTHF are slightly lower than those in 1M $LiPF_6$-2MeTHF (Fig. S2c-d). Haven ratio is the ratio of conductivity calculated from diffusion coefficients using the Nernst-Einstein equation to the measured conductivity(1). Due to the presence of dynamic ion-ion correlations, the Haven ratio of practical electrolytes is generally larger than 1. At ambient temperature, the Haven ratios of 1M LiFSI-2MeTHF and 1M $LiPF_6$-2MeTHF are 8.3 and 17.3, respectively. Such high Haven

ratios indicate that the Li^+ and anion form ion pairs and clusters in these two electrolytes, leading to the Li^+ and the anion diffusing at nearly identical rates.

Table S1. Conductivities and diffusion coefficient of Li^+ in $LiPF_6$- and LiFSI-based electrolytes.

	Diffusion Coefficient (20°C, m^2/s)[1]	Conductivity (20°C, mS/cm)[2]	Diffusion Coefficient (-20°C, m^2/s)[1]	Conductivity (-20°C, mS/cm)[2]
$LiPF_6$	4.46E-10	1.94	1.90E-10	1.41
LiFSI	3.74E-10	3.43	1.52E-10	2.35

[1,2] the data come from NMR measurements.

Table S2. Parameters of graphite laminate (provided by the CAMP Facility at Argonne National Laboratory)

Thickness	Porosity	Mass loading	Active materials	Inactive materials	Density
55µm	34.6%	6.38 mg/cm^2	91.83%	8.17%	1.42 g/cm^3

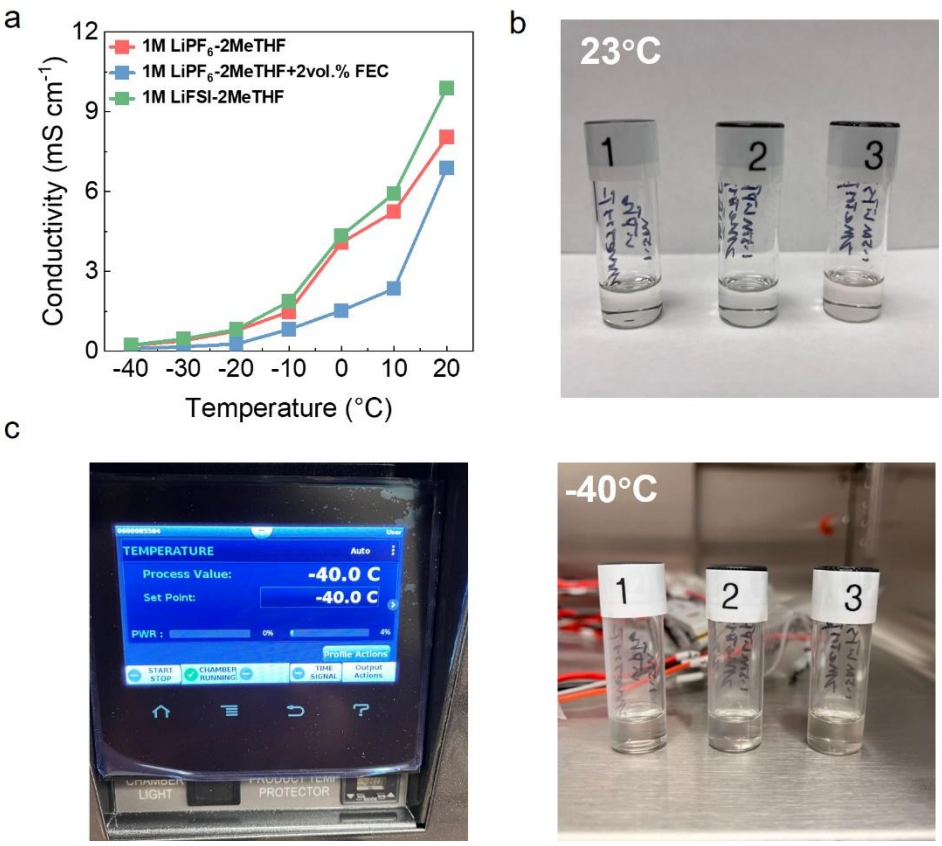

Fig. S3. **a**, Ionic conductivities of the three electrolytes in the temperature range from 20 to -40 °C (measured in a coin cell, details shown in the experimental section). **b, c**, the photos of the electrolytes stored at 23°C and -40°C, which are all clear and transparent and do not freeze. **1**: 1M $LiPF_6$-2MeTHF, **2**: 1M $LiPF_6$-2MeTHF+2vol.% FEC, **3**:1M LiFSI-2MeTHF.

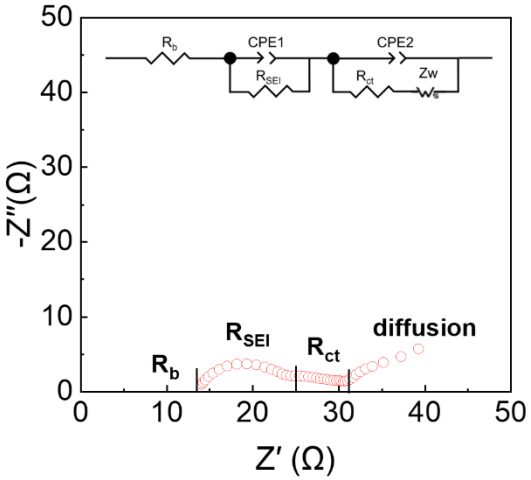

Fig. S4. The electrochemical impedance spectrum (EIS) of the Gr||Li cell after full lithiation. The equivalent circuit shows the corresponding resistance of R_b, R_{SEI}, and R_{ct}.

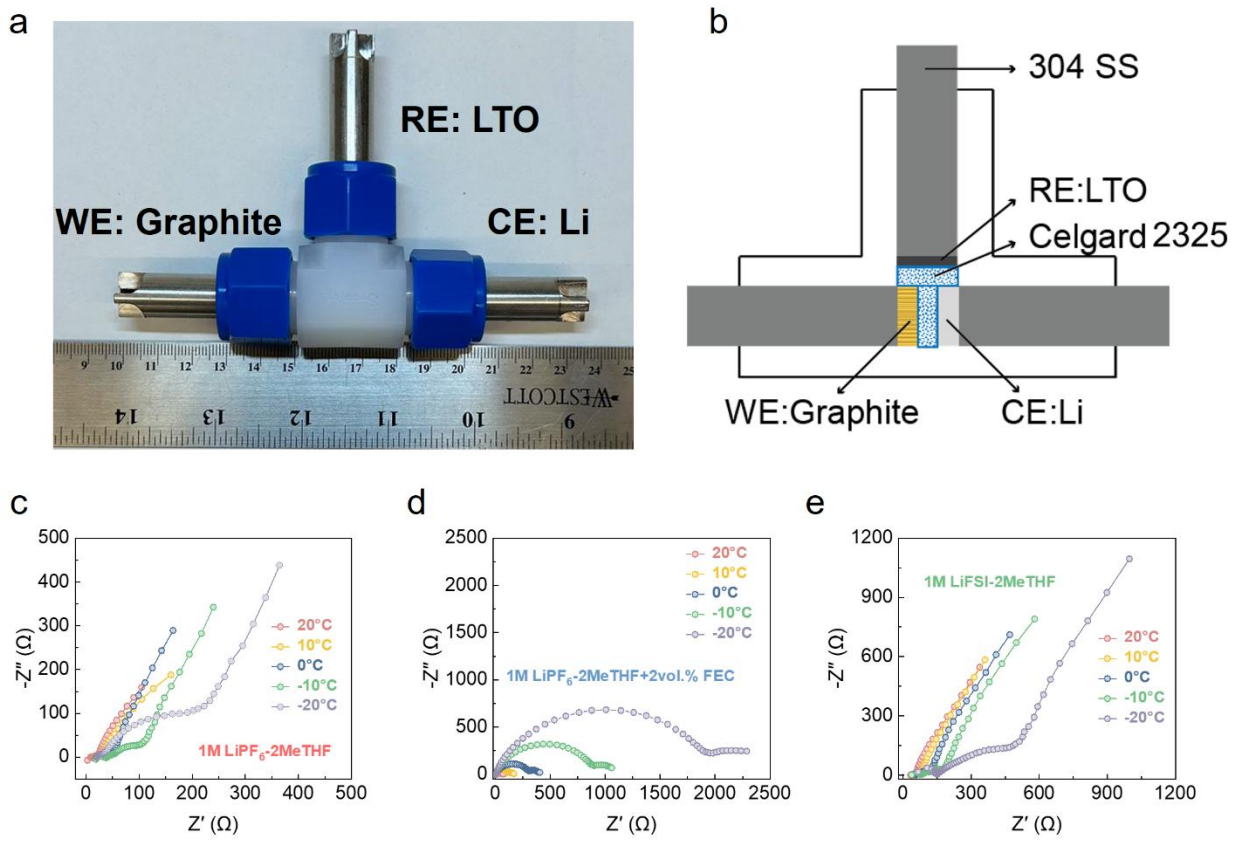

Fig. S5. **a**, Customized three-electrode cell and (**b**) the setup for the EIS test. Temperature-dependent electrochemical impedance spectroscopy of the Gr||Li cell at 50% SOC after 5 cycles in the: **c**, 1M $LiPF_6$-2MeTHF electrolyte; **d**, 1M $LiPF_6$-2MeTHF+2vol.% FEC electrolyte; **e**, 1M LiFSI-2MeTHF electrolyte.

Table S3. The fitted impedances of the three-electrode cell cycled in different electrolytes from 20 to -20°C.

Electrolyte / Temperature	1M $LiPF_6$-2MeTHF			1M $LiPF_6$-2MeTHF+2vol.% FEC			1M LiFSI-2MeTHF		
	R_b	R_{SEI}	R_{ct}	R_b	R_{SEI}	R_{ct}	R_b	R_{SEI}	R_{ct}
20°C	4.2	6.7	15.8	4.8	49.5	25.2	8.2	10.2	15.7
10°C	6.8	11.0	24.6	7.1	119.4	64.4	18.1	21.5	23.8
0°C	9.0	21.4	51.1	12.8	290.4	125.1	27.3	45.6	66.9
-10°C	13.1	36.1	106.7	38.3	846.1	254.3	45.1	80.9	165.4
-20°C	23.9	65.3	235.3	153.8	1662.5	422.4	135.8	156.7	328.3

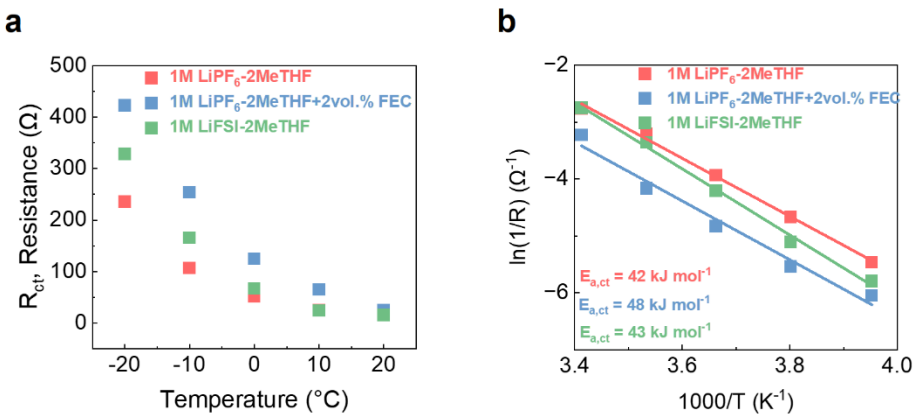

Fig. S6. a, Fitting results of R_{ct} evolution at different temperatures. **b**, Arrhenius plots and activation energies of R_{ct} derived from temperature-dependent EIS measurements.

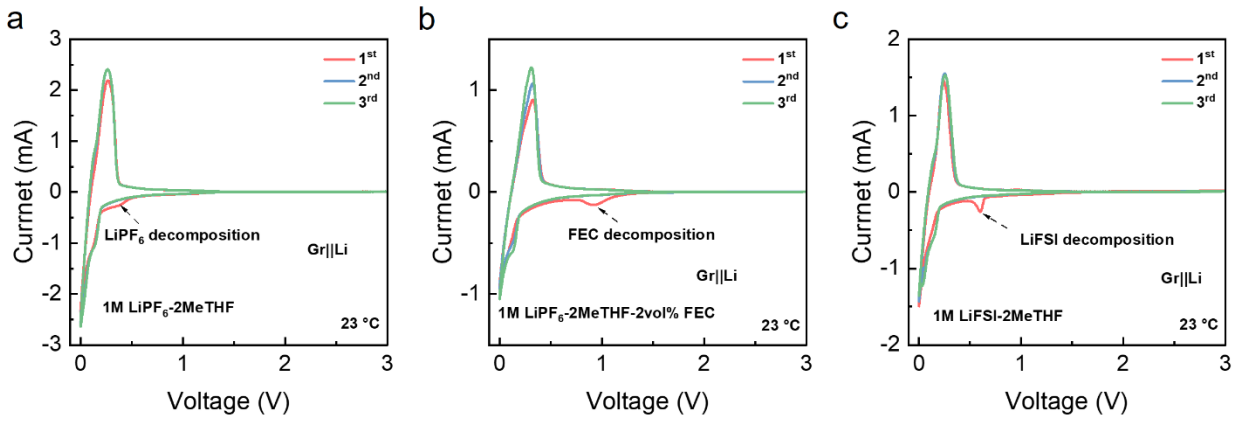

Fig. S7. CV curves of the graphite||Li cell cycled in the: **a**, 1M $LiPF_6$-2MeTHF electrolyte; **b**, 1M $LiPF_6$-2MeTHF+2vol.% FEC electrolyte; **c**, 1M LiFSI-2MeTHF electrolyte.

The decomposition products of FEC additives, LiFSI, and $LiPF_6$ salts:

Due to the characteristics of weakly solvating electrolytes, the formation of the SEI layer is primarily attributed to the decomposition of FEC additives and Li salts. FEC is one of the most popular electrolyte additives for tailoring SEI properties in Li-ion batteries. As a film-forming additive, FEC has a high dielectric constant and tends to accumulate on the electrode surface, promoting the formation of a thicker and denser SEI layer(2–4)During the early stages of lithiation, the cleavage of the C-F bond in FEC increases the LiF content within the SEI layer. Simultaneously, the unstable carbonate ring structure undergoes a ring-opening reaction, rupturing one of its C-O bonds to form an intermediate containing a fluoroalkyl group and a carbonate ion. The final products are LiF, Li_2CO_3, and organic species ($R\text{-}OCO_2Li$).

The poor reduction stability of the LiFSI salt also causes it to begin decomposing during the early lithiation stage, leading to the formation of a dense SEI layer rich in LiF(5). During this decomposition process, the S-F bond in LiFSI breaks, generating N-containing intermediates and LiF. Meanwhile, the S-N and S=O bond in the intermediates also breaks, with the final products being LiF, Li_2O, SO_2F, Li_3N, and organic species(6, 7).

$LiPF_6$ salt has different reduction products and decomposition pathways. $LiPF_6$ can generate LiF through both chemical and electrochemical pathways. It has relatively poor chemical stability and can produce LiF when reacting with moisture(8). In terms of the electrochemical pathway, the decomposition of $LiPF_6$ is the result of the combined action of direct anion reduction and electrocatalytic transformation from HF(9). Due to the following well-known instability of H_2O-containing organic $LiPF_6$ solutions: $LiPF_6 \rightarrow LiF+PF_5$; $PF_5+H_2O \rightarrow POF_3+2HF$, HF is thus generated. In the 1M $LiPF_6$-2MeTHF electrolyte, we speculate that a trace amount of HF exists and is likely to be distributed throughout the anode surface. Therefore, LiF nucleates via the electrocatalytic transformation of HF, followed by significant anion reduction. The final products are LiF, Li_2O, PO_xF_y, and organic species.

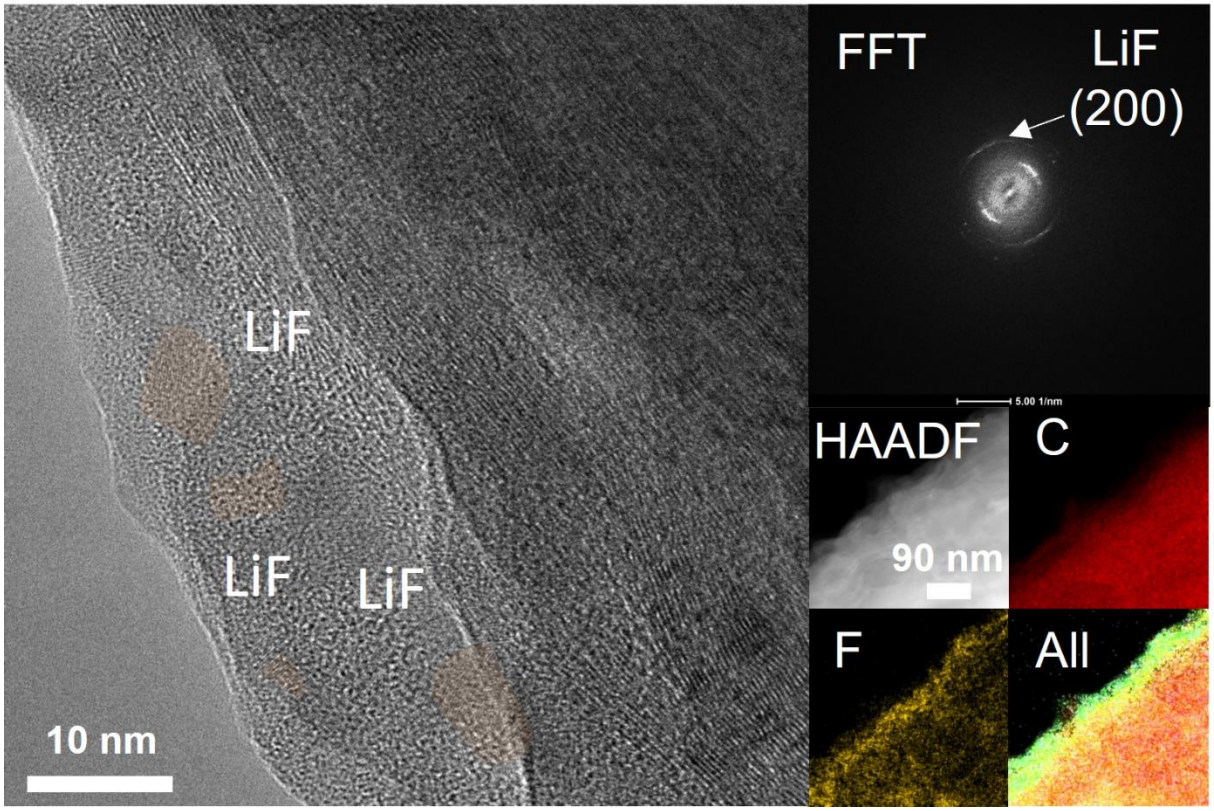

Fig. S8. Cryo-TEM images of the graphite electrode cycled using (**a**) 1M LiFSI-2MeTHF electrolyte for 20 cycles, including the corresponding fast Fourier transform patterns and STEM-EDS elemental mapping of F, C, and all elements overlaid in one image.

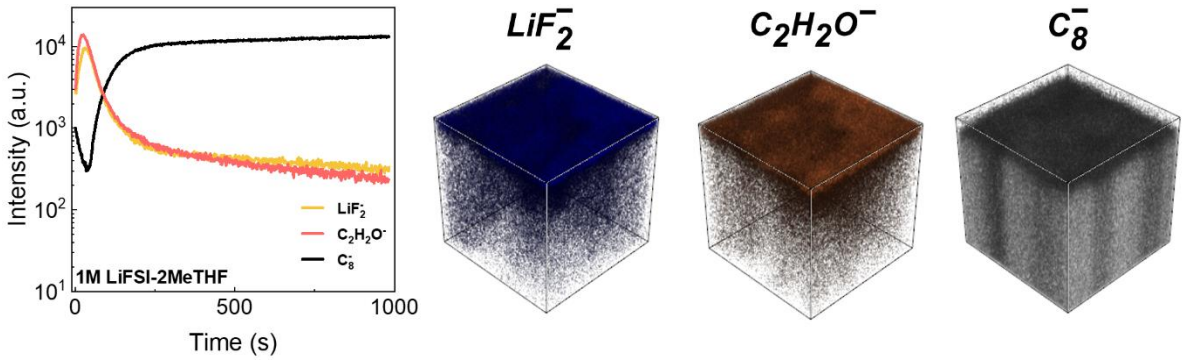

Fig. S9. TOF-SIMS depth profiles of various chemical species for the graphite anode using 1M LiFSI-2MeTHF electrolyte after 20 cycles: 3D maps showing the distribution of several molecular fragments: LiF_2^-, $C_2H_2O^-$, and C_8^- in the cycled graphite, where the sample volume is a 100×100 μm area with a 100 nm depth.

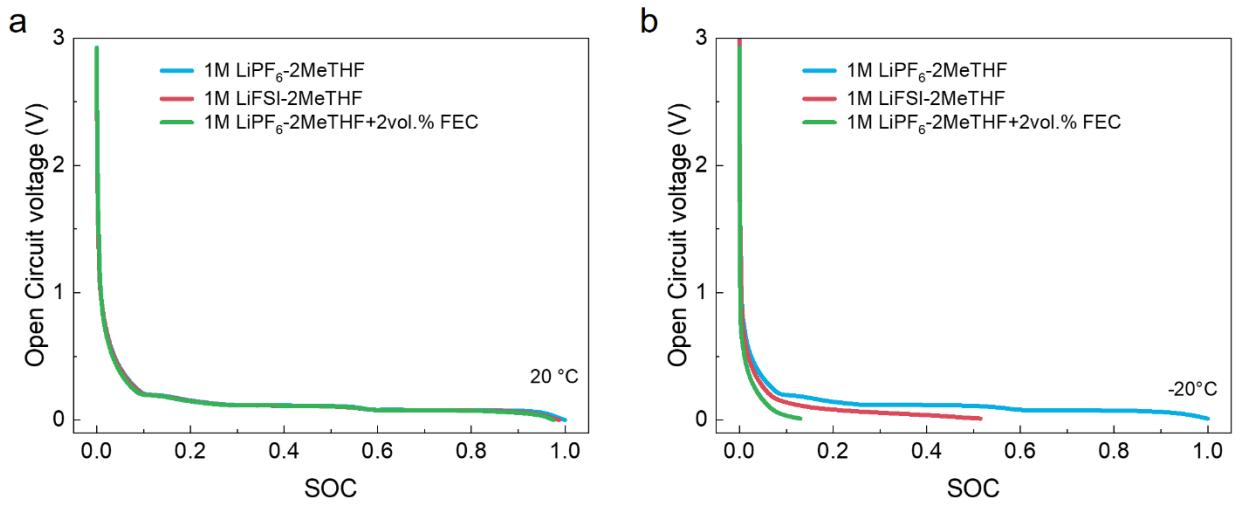

Fig. S10. The equilibrium voltage (measured at C/20) of the Gr anode cycled in three electrolytes at different temperatures: a, 20°C. b, -20°C.

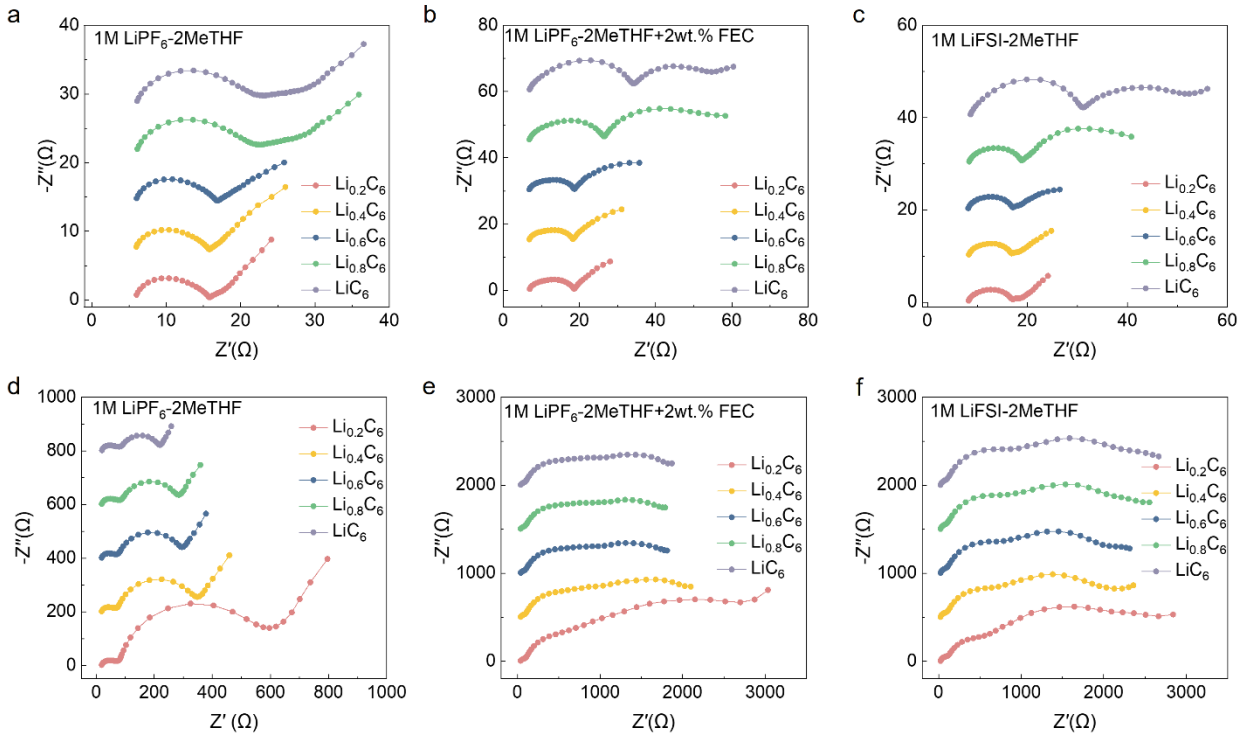

Fig. S11. The electrochemical impedance spectrum (EIS) of the Gr||Li cell cycled in three electrolytes at different lithiation stages at 23°C, and -20°C, respectively. (a-c): cycled at 0.2 C at 23°C; (d-f) cycled at 0.2 C at -20°C.

Table S4. The fitted impedances of the Gr||Li two-electrode cells cycled in different electrolytes at 0.2C at 23°C.

Gr||Li	1M $LiPF_6$-2MeTHF			1M $LiPF_6$-2MeTHF+2vol.% FEC			1M LiFSI-2MeTHF		
Lithiation degree	R_b	R_{SEI}	R_{ct}	R_b	R_{SEI}	R_{ct}	R_b	R_{SEI}	R_{ct}
0.2	5.4	9.5	3.1	6.5	12.3	9.9	7.9	9.1	1.2
0.4	5.7	4.9	4.9	6.4	12.1	16.3	8.0	8.8	0.38
0.6	5.8	6.5	3.9	6.4	12.4	21.1	7.9	8.9	34.2
0.8	5.4	13.5	10.6	6.4	20.1	26.4	8.0	9.4	28.6
1.0	5.4	13.7	11.0	6.5	28.1	16.3	8.3	22.8	18.0

Table S5. The fitted impedances of the Gr||Li two-electrode cells cycled in different electrolytes at 0.2C at -20°C.

Gr||Li	1M $LiPF_6$-2MeTHF			1M $LiPF_6$-2MeTHF+2vol.% FEC			1M LiFSI-2MeTHF		
Lithiation degree	R_b	R_{SEI}	R_{ct}	R_b	R_{SEI}	R_{ct}	R_b	R_{SEI}	R_{ct}
0.2	16.9	46.2	372.6	14.6	2293	172.6	15.6	474	2566
0.4	17.2	47.9	232.4	19.0	1297	225	16.5	1600	598
0.6	17.5	52.7	199.2	18.3	1238	226	17.2	1646	505
0.8	17.8	62.8	186.9	18.4	1229	223	17.4	1706	652
1.0	18.4	60.8	136.2	18.4	1308	236	17.5	1759	705

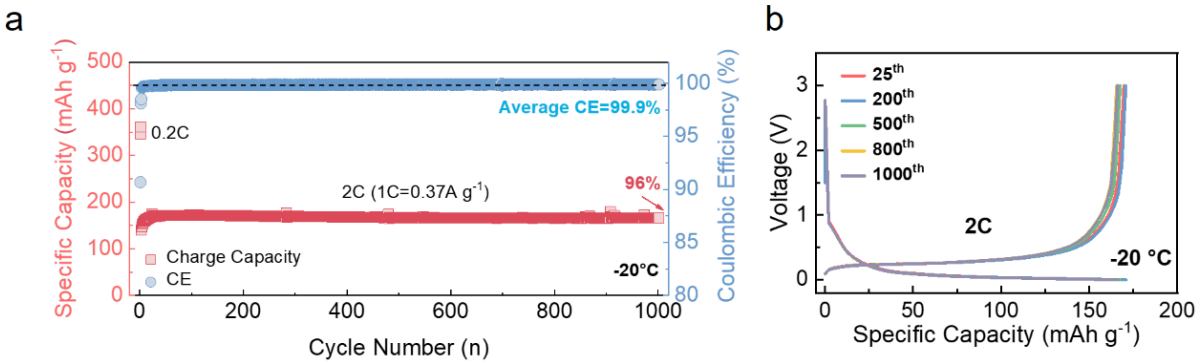

Fig. S12. a, Long-term cycling performance of the Gr||Li cell cycled in the 1M $LiPF_6$-2MeTHF electrolyte at 2C under -20°C. b, Voltage profiles of the Gr||Li cells shown in (a) at 2C under -20°C.

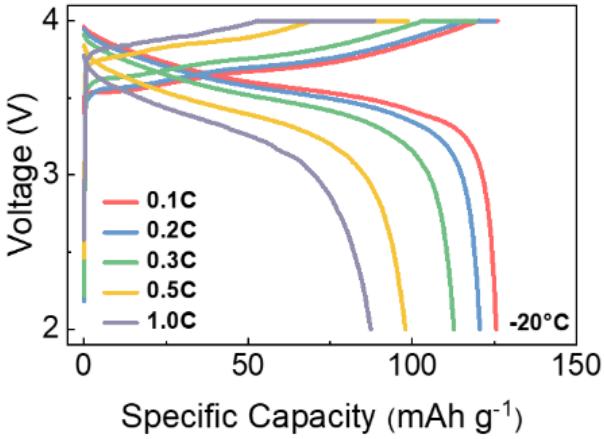

Fig. S13. Voltage profiles of the Gr||NMC622 cell shown in (Fig. 4g) at current density from 0.1 to 1.0C (1C=0.18A g^{-1}) at -20°C.

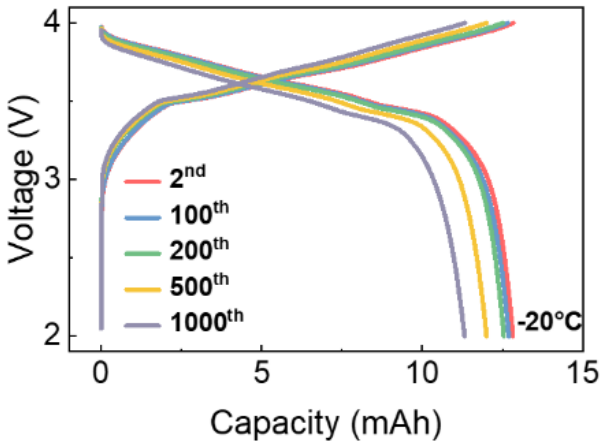

Fig. S14. Voltage profiles of the Gr||NMC622 cell shown in (Fig. 5h) at 0.2C (1C=0.18A g^{-1}) under -20°C.

References

1. D. Yu, *et al.*, Uncorrelated Lithium-Ion Hopping in a Dynamic Solvent-Anion Network. *ACS Energy Lett.* **8**, 1944–1951 (2023).

2. Q. Wu, M. T. Mcdowell, Y. Qi, Effect of the Electric Double Layer (EDL) in Multicomponent Electrolyte Reduction and Solid Electrolyte Interphase (SEI) Formation in Lithium Batteries. *J. Am. Chem. Soc* **145,** 2473-2484 (2023).

3. B. Han, *et al.*, Additive stabilization of SEI on graphite observed using cryo-electron microscopy. *Energy Environ. Sci.* **14**, 4882–4889 (2021).

4. T. Hou, *et al.*, The influence of FEC on the solvation structure and reduction reaction of $LiPF_6$/EC electrolytes and its implication for solid electrolyte interphase formation. *Nano Energy* **64**, 103881 (2019).

5. Y. Aoki, *et al.*, Effective Approach by Computational Chemical Prediction and Experimental Verification to Elucidate SEI Formation Mechanism in $LiPF_6$-, LiFSI-, and $LiBF_4$-Containing Electrolyte Solutions. *J. Phys. Chem. C* **127**, 69–77 (2023).

6. T. Li, *et al.*, Stable Anion-Derived Solid Electrolyte Interphase in Lithium Metal Batteries. *Angew. Chem. Int. Ed.* **60**, 22683–22687 (2021).

7. W. Yu, *et al.*, Electrochemical formation of bis(fluorosulfonyl)imide-derived solid-electrolyte interphase at Li-metal potential. *Nat. Chem.* 1–10 (2024). https://doi.org/10.1038/s41557-024-01689-5.

8. A. Wang, S. Kadam, H. Li, S. Shi, Y. Qi, Review on modeling of the anode solid electrolyte interphase (SEI) for lithium-ion batteries. *npj Comput. Mater.* **4**, 15 (2018).

9. C. Cao, *et al.*, Toward Unraveling the Origin of Lithium Fluoride in the Solid Electrolyte Interphase. *Chem. Mater.* **33**, 7315–7336 (2021).